# Paleoenvironmental changes in the northern South China Sea over the past 28,000 years: a study of $TEX_{86}$-derived sea surface temperatures and terrestrial biomarkers

Tomoya Shintani[1,2], Masanobu Yamamoto [1,3,*] and Min-Te Chen[4]

[1]Graduate School of Environmental Science, Hokkaido University, Kita-10, Nishi-5, Kita-ku, Sapporo 060-0810, Japan.

[2]Present address: CHINO Corporation, 32-8, Kumano-cho, Itabashi-ku, Tokyo 173-8632, Japan.

[3]Faculty of Environmental Earth Science, Hokkaido University, Kita-10, Nishi-5, Kita-ku, Sapporo 060-0810, Japan.

[4]Institute of Applied Geosciences, National Taiwan Ocean University, Keelung 20224, Taiwan.

*Corresponding author: E-mail: myama@ees.hokudai.ac.jp

Keywords: South China Sea, $TEX_{86}$, $U^{K'}_{37}$, paleotemperature, biomarkers, terrestrial organic matter, Late Quaternary

Abstract: We have generated a record of $TEX_{86}$ ($TEX_{86}^{H}$)-derived sea surface temperatures (SSTs) over the last 28 ka for core MD97-2146 from the northern South China Sea (SCS). The $TEX_{86}^{H}$-derived temperature of a core-top sample corresponds to the SSTs in warmer seasons. The SST record shows a drop during the Oldest Dryas period, an abrupt rise at the

onset of the Bølling-Allerød period, a plateau across the Younger Dryas period, and an abrupt rise at the beginning of the Holocene. The glacial–interglacial contrast in $TEX_{86}^{H}$-derived temperature is almost the same as that in foraminiferal Mg/Ca ratio-derived temperature, but it is larger than those in $U_{37}^{K'}$ and transfer function-derived temperatures. Possible interpretations are 1) the seasonal shift of glycerol dialkyl glycerol tetraether (GDGT) production, 2) the overestimation of temperature change by $TEX_{86}^{H}$, and 3) the underestimation of temperature change by $U_{37}^{K'}$ and transfer function approaches. The similar variation in $TEX_{86}^{H}$-derived temperature at the study site and Chinese stalagmite $\delta^{18}O$ during the last deglaciation suggests that changes in $TEX_{86}^{H}$-derived temperature in this period reflected atmospheric and oceanic reorganization on a millennial timescale. The long-chain n-alkanes are mainly of higher plant origin before ~14 ka and a mixture of higher plant and lithic origins after ~14 ka; the abundance ratio of long-chain to short-chain n-fatty acids decreases at ~15 ka, suggesting a drastic change in sediment sources at ~14–15 ka. We attribute the higher content of fresh higher plant n-alkanes and long-chain n-fatty acids before ~14–15 ka to enhanced aeolian transportation and/or arid environments. Increased precipitation likely due to intensified summer monsoon after ~14–15 ka enhanced the erosion of sedimentary rocks and increased the contribution of lithic n-alkanes.

## 1. Introduction

Numerous paleoceanographic studies of sea surface temperature (SST) have been undertaken in the South China Sea (SCS). Wang and Wang (1990) and Wang et al. (1995) generated summer and winter SST records for the SCS, based on foraminifer assemblages, and found that during the last glacial maximum (LGM) the SCS experienced larger

seasonal SST differences and a steeper latitudinal SST gradient than it does presently. Similar phenomena were reported using foraminifer- and alkenone-based SST records for the northern SCS (Huang et al., 1997a, b; Chen and Huang, 1998; Pelejero et al., 1999a; Chen et al., 2003). Kienast et al. (2001) identified a millennium-scale temperature variation that mimics Greenland ice core records. Recently, Oppo and Sun (2005) and Zhao et al. (2006) reported millennium-scale temperature records from the northern and southern SCS, respectively, for the time since the penultimate glacial interval. The glacial–interglacial changes of SST in the SCS have been attributed either to the inflow of cold water from the North Pacific (e.g., Wang and Wang, 1990; Wang et al., 1995) or to changes in winter monsoon intensity (e.g., Huang et al., 1997a, b). Disagreements of paleotemperatures in the SCS among different proxies such as alkenone $U^{K'}_{37}$, the foraminiferal Mg/Ca ratio, and transfer function are potentially attributable to differences in the season and depth that each proxy reflects (e.g., Steinke et al., 2008). Alternative approaches are useful for better understanding paleotemperature changes in the SCS.

$TEX_{86}$ is a recently developed paleotemperature proxy (Schouten et al., 2002), which is based on glycerol dialkyl glycerol tetraethers (GDGTs). The $TEX_{86}$ paleothermometer has the advantage that it does not seem to be influenced by changes in salinity (Wuchter et al., 2004) and is more sensitive to temperature changes in tropical waters (Kim et al., 2010). However, caution is still required when applying $TEX_{86}$ because a water-column study suggested that $TEX_{86}$ recorded not only temperature changes, but also changes in archaeal ecology, nutrient concentrations, and possibly oceanographic conditions (Turich et al., 2007). More case studies are necessary to test the reliability of this proxy. Furthermore, $TEX_{86}$ has not been previously applied to SCS sediments.

Changes in terrestrial vegetation and sediment transport pathways have also been

investigated from the perspective of monsoon variation. Sun and Li (1999) reported a transition from a herb-dominated cool and dry climate during the last glacial to a warm and humid climate in the Holocene in south China, as shown by pollen and spore assemblages in the SONNE 17940 core from the northern SCS. Wang et al. (1999a) attributed the increase in clay content observed at ~14.5 ka in core 17940 to an increase in fluvial supply from the Pearl River due to the intensification of the summer monsoon. Pelejero (2003) revealed the parallel glacial–interglacial variability of terrestrial n-alkane concentration in four different cores retrieved from the northern, western and southern SCS, taking values linearly inversely correlated to the $U^{K'}_{37}$-derived SST, with higher concentrations during glacials. This oscillation was attributed to the emergence and flooding of the shelves caused by sea level variations, together with SCS SSTs, have a clear dependency on the Northern Hemisphere climate evolution. Terrestrial biomarkers such as long-chain n-alkanes and long-chain n-fatty acids are useful for understanding the contribution and provenance of terrestrial material (e.g., Pelejero et al., 1999b; Pelejero, 2003; Yamamoto and Polyak, 2009).

This study presents records of $TEX_{86}^{H}$-derived SSTs and terrestrial biomarkers for the last 28,000 years from northern SCS core MD97-2146, located offshore from southern China. The objective of this work is to understand changes in SSTs derived from $TEX_{86}^{H}$ as well as changes in sediment provenance. This is the first report of the application of $TEX_{86}$ ($TEX_{86}^{H}$) paleothermometry in the SCS.

## 2.Oceanographic settings

The SCS is a marginal sea of the North Pacific with seven connections to surrounding seas and oceans (Fig. 1): the Taiwan Strait to the East China Sea (sill depth ~70 m), the

Bashi Strait to the North Pacific (sill depth ~2500 m), the Mindoro and Balabac Straits to the Sulu Sea (sill depths ~450 and ~100 m, respectively), the Malacca Strait to the Indian Ocean (sill depth ~30 m), and the Gaspar and Karimata Straits (~40-50 m) to the Java Sea (Wyrtki, 1961). Surface circulation in the SCS is driven by large-scale, seasonally-reversed monsoon winds (Wyrtki, 1961). In the boreal summer, southwesterly winds drive an inflow of Indian Ocean water through the Sunda Shelf and a clockwise surface circulation in the SCS. In the boreal winter, northeasterly winds drive an inflow of North Pacific and East China Sea waters through the Bashi and Taiwan Straits, and surface circulation in the SCS is counterclockwise.

## 3. Materials and Methods

### *3.1. Samples and age-depth model*

During the IMAGES 1997 *Marion Dufresne* cruise, a giant piston core (MD97-2146; 38.69 m long) was collected from a water depth of 1720 m on the northern slope of the SCS at 20°07.08'N, 117°23.02'E (Fig. 1). The sediment retrieved consisted of dark gray nannofossil and foraminifer oozes with some radiolarians and diatoms (Chen et al., 1998).

An age model in calendar years was created from the AMS $^{14}$C ages of seven samples of the planktonic foraminiferan *Globigerinoides sacculifer* (Lin et al., 2006) and six samples of mixed planktonic foraminifera *Globigerinoides ruber* and *G. sacculifer* (Shintani et al., 2008). The calendar age was converted using the CALIB5.0 program and marine04.14C dataset (Reimer et al., 2004) with a 400-year global reservoir correction (Shintani et al., 2008). Lin et al. (2006) created an age model using a combination of $^{14}$C ages and stratigraphic correlation with nearby core 17940 (Wang et al., 1999b). The present work does not use any stratigraphic correlation, however, because the assumption that

121 temperatures in core 17940 changed synchronously with Greenland temperatures (Wang et
122 al., 1999b) is not necessary.
123 A total of 76 samples were collected every 20 cm on average (equivalent to
124 approximately 300-year intervals) down to a depth of 19 m (0-28 ka).
125
126 *3.2 Hydrocarbon analysis*
127 Lipids were extracted (x 2) from 1 g of dried sediment using a DIONEX Accelerated
128 Solvent Extractor ASE-200 at 100°C and 1000 psi for 10 min with 11 ml of
129 $CH_2Cl_2$–$CH_3OH$ (6:4) and then concentrated. The lipid extract was separated into four
130 fractions using column chromatography ($SiO_2$ with 5% distilled water; i.d., 5.5 mm; length,
131 45 mm): F1 (hydrocarbons), 3ml hexane; F2 (aromatic hydrocarbons), 3 ml hexane-toluene
132 (3:1); F3 (ketones), 4 ml toluene; F4 (polar compounds), 3 ml toluene–$CH_3OH$ (3:1);
133 *n*-$C_{24}D_{50}$ and *n*-$C_{36}H_{74}$ were added as internal standards to F1 and F3, respectively.
134 An aliquot of F4 was trans-esterified with 1 ml 5% HCl–$CH_3OH$ at 60˚C for 12 h
135 under $N_2$. The esterified lipids were supplemented with 2 ml distilled water and extracted
136 (x 3) with toluene. The extract was back-washed (x 3) with distilled water, passed through
137 a short bed of $Na_2SO_4$, and separated into two fractions with $SiO_2$ column chromatography:
138 F4-1 (acids), 4 ml toluene; F4-2 (alcohols), 3 ml toluene-$CH_3OH$ (3:1); *n*-$C_{24}D_{50}$ was
139 added as an internal standard to F4-1.
140 Gas chromatography (GC) was conducted using a Hewlett Packard 5890 series II gas
141 chromatograph with on-column injection and electronic pressure control systems, and a
142 flame ionization detector (FID). Samples were dissolved in hexane. Helium was the carrier
143 gas and the flow velocity was maintained at 30 cm/s. A Chrompack CP-Sil5CB column
144 was used (length, 60 m; i.d., 0.25 mm; thickness, 0.25 μm). The oven temperature was

programmed to rise from 70 to 130˚C at 20˚C/min, from 130 to 310˚C at 4˚C/min, and to hold at 310˚C for > 30 min. The standard deviations of five duplicate analyses averaged 7.5% of the concentration for each compound.

Gas chromatography-mass spectrometry (GC-MS) of F1, F3 and F4-1 was conducted using a Hewlett Packard 5973 GC-mass selective detector with on-column injection and electronic pressure control systems, and a quadrupole mass spectrometer. The GC column and oven temperature and carrier pressure programs were as described above. The mass spectrometer was run in full scan mode (*m/z* 50−650). Electron ionization (EI) spectra were obtained at 70 eV. Compound identification was achieved by comparing mass spectra and retention times with those of standards and published data.

*3.3 Glycerol dialkyl glycerol tetraether (GDGT) analysis*

An aliquot of F4-2 was dissolved in hexane–2-propanol (99:1) and filtered. Glycerol dialkyl glycerol tetraethers (GDGTs) were analyzed using high performance liquid chromatography-mass spectrometry (HPLC-MS) with an Agilent 1100 HPLC system connected to a Bruker Daltonics micrOTOF-HS time-of-flight mass spectrometer. Separation was conducted using a Prevail Cyano column (2.1 x 150 mm, 3µm; Alltech) and maintained at 30˚C following the method of Hopmans et al. (2000) and Schouten et al. (2007). Conditions were: flow rate 0.2 ml/min, isocratic with 99% hexane and 1% 2-propanol for the first 5 min followed by a linear gradient to 1.8% 2-propanol over 45 min. Detection was achieved using atmospheric pressure, positive ion chemical ionization-mass spectrometry (APCI-MS). The spectrometer was run in full scan mode (*m/z* 500−1500). Compounds were identified by comparing mass spectra and retention times with those of GDGT standards (formed from the main phospholipids of *Thermoplasma acidophilum* via

169 acid hydrolysis) and those in the literature (Hopmans et al., 2000). Quantification was
170 achieved by integrating the summed peak areas in the $(M+H)^+$ and the isotopic $(M+H+1)^+$
171 ion traces.

172 $TEX_{86}^H$ was calculated from the concentrations of GDGT-1, GDGT-2, GDGT-3 and a
173 regioisomer of crenarchaeol using the following expression (Schouten et al., 2002; Kim et
174 al., 2010):

175

176 $TEX_{86}^H = \log TEX_{86} = \log ([GDGT\text{-}2]+[GDGT\text{-}3]+[Crenarchaeol\ regioisomer])/$
177 $([GDGT\text{-}1]+[GDGT\text{-}2]+[GDGT\text{-}3]+[Crenarchaeol\ regioisomer])$

178

179 $TEX_{86}^H$ is defined as the logarithmic function of $TEX_{86}$ and yields the best correlation with
180 SST when the data from polar and subpolar oceans are removed (Kim et al., 2010).
181 Temperature was calculated according to the following equation based on a global core-top
182 calibration (Kim et al., 2010):

183

184 $$T = 68.4 \times TEX_{86}^H + 38.6$$

185

186 where T = temperature [°C]; analytical accuracy was 0.45°C in our laboratory.

187

188 **4. Results**

189 *4.1.* $TEX_{86}^H$

190 The $TEX_{86}^H$-derived temperature profile indicates that between 18 and 28 ka SSTs were
191 nearly constant at 23.3°C, decreased to 20.8°C at 16.7 ka, and then increased abruptly to
192 25.8°C by 14.5 ka. After 14.5 ka SSTs increased gradually to 26.3°C by 12.9 ka, and then

193 decreased to 25.4°C at 12.3 ka, before increasing abruptly to 28.0°C by 11.0 ka. After 11.0
194 ka SSTs increased gradually to 28.7°C by 5.3 ka and remained constant thereafter (Fig. 3A).
195 The core-top temperature was 28.1°C. This temperature is higher than the mean annual
196 SST (26.6°C; NOAA, 1998) and agrees with the SST in May and September-October at
197 this site (~28.0°C and ~27.7-28.6°C, respectively; NOAA, 1998).
198 The Branched and Isopernoid Tetraether (BIT) index, a proxy for soil versus marine
199 organic matter input to sediments (Hopamans et al, 2004), was constantly low (< 0.03).
200
201 *4.2. Normal alkanes*
202 Normal alkanes (n-alkanes) occur as a major component of the F1 (hydrocarbon)
203 fraction and show a unimodal distribution with a maximum at $C_{31}$. The total concentration
204 of long-chain $C_{25}$-$C_{33}$ n-alkanes varies between 0.41 and 1.66 μg/g in sediment, with an
205 average of 0.86 μg/g (Fig. 4A). The odd carbon number preference index (CPI) values of
206 $C_{24}$-$C_{34}$ homologues (Bray and Evans, 1961) vary between 2.0 and 6.2, with an average of
207 3.4. The average chain length (ACL) values of $C_{27}$-$C_{33}$ homologues (Bray and Evans,
208 1961) vary between 29.1 and 30.3, with an average of 29.7.
209 Most samples showed the n-alkane distribution as a mixture of a pattern with high odd
210 carbon number preference (CPI > ~5; Fig. 4A) and a pattern heavily influenced by mature
211 (thermally altered) n-alkane with low CPI values (~2.5; Fig. 4A). The former is typical of
212 terrestrial higher plant waxes (Eglinton and Hamilton, 1967). This pattern indicates that the
213 OM was derived from fresh higher plant material. The latter is typical of coal and coaly
214 shale (Bray and Evans, 1961), indicating an influx of mature (lithic) OM.
215 If we assess the end-member CPI values of higher plant and mature OM, we can
216 estimate the concentrations of n-alkanes of both origins. Assuming that the long-chain

n-alkanes derived from higher plant waxes have CPI values of 6.2 (maximal value for samples in the study core), and that those derived from mature rocks have CPI values of 1 (typical values of OM in catagenesis and metagenesis stages; Tissot and Welte, 1984), we calculated concentrations of "higher plant" and "lithic" $C_{25}$-$C_{33}$ n-alkanes from the total $C_{25}$-$C_{33}$ n-alkane concentration and the CPI value using the following formulae (Yamamoto and Polyak, 2009):

Higher plant $C_{25}$-$C_{33}$ n-alkane

$= \text{total } C_{25}\text{-}C_{33} \text{ n-alkane} \times \{(6.2+1)\,(CPI-1)\}/\{(6.2-1)(CPI+1)\}$

Lithic $C_{25}$-$C_{33}$ n-alkane = total $C_{25}$-$C_{33}$ n-alkane – higher plant $C_{25}$-$C_{33}$ n-alkane

The concentration of higher plant long-chain n-alkanes varies between 0.29 and 1.33 μg/g with an average of 0.64 μg/g. The concentration of lithic long-chain n-alkanes varies between 0 and 0.55 μg/g with an average of 0.23 μg/g. Both total and higher plant n-alkanes show a similar pattern over the last 30 kyr: they are higher between 14 and 30 ka than between 2 and 14 ka, and increase to present-day values at around 2 ka (Fig. 4A). In contrast, lithic n-alkanes remain low until 15 ka, increased at 15 ka, and then increase gradually thereafter (Fig. 4A).

*4.3. Normal fatty acids*

Normal fatty acids (n-fatty acids) occur as a major component of the F4-1 (acid) fraction and show a bimodal distribution with a maximum at $C_{16}$ and $C_{26}$ or $C_{28}$. Short-chain n-fatty acids are ubiquitous in eukaryotes and bacteria, while long-chain n-fatty acids are specific to higher plants (Kvenvolden et al., 1967). The even CPI values of

241 $C_{25}$-$C_{33}$ homologues (Kvenvolden et al., 1967) were nearly constant with a range of
242 between 3.6 and 4.8 and an average of 4.2 (Fig. 4B).

243 The total concentration of n-fatty acids ($C_{14}$-$C_{34}$) varies between 5.9 and 34.5 μg/g,
244 with an average of 10.7 μg/g (Fig. 4B). The concentration of short-chain n-fatty acids
245 ($C_{14}$-$C_{18}$) varies between 1.3 and 12.1 μg/g, with an average of 3.6 μg/g (Fig. 4B). The
246 concentration of long-chain n-fatty acids ($C_{26}$-$C_{34}$) varies between 2.3 and 13.4 μg/g, with
247 an average of 4.7 μg/g. The concentration of short-chain n-fatty acids was constant with the
248 exception of a peak at 17.3 ka, while the concentration of long-chain n-fatty acids shows
249 several peaks prior to 15 ka (Fig. 4B).

250

251 **5. Discussion**

252 *5.1. SST changes*

253 The $U^{K'}_{37}$-derived temperature in this core was reported by Shintani et al. (2008).
254 Temperature records were calculated using the equations of Prahl et al. (1988). The SSTs
255 fluctuated slightly between 28–16 ka but maintained an average of 24.0°C. By 14.8 ka,
256 SSTs increased to 24.7°C, whereupon they remained constant until 10.7 ka. After 10.7 ka
257 SSTs increased to 26.5°C by 6.1 ka and then increased more gradually to reach 27°C at
258 present (Fig. 3B). This variation is similar to that recorded in nearby core 17940 (Pelejero
259 et al., 1999a). Present-day SST at the study site shows a seasonal variation between 23.7°C
260 in January and 28.9°C in July, with a mean annual value of 26.6°C (Fig. 2; NOAA, 1998).
261 The $U^{K'}_{37}$-derived core-top temperature is 26.0°C. This temperature is slightly lower than
262 the mean annual SST at this site (26.6°C; NOAA, 1998). As indicated from satellite
263 observations, chlorophyll concentrations do not display large seasonal variations, with only
264 a moderate maximum in the winter season in the study area (Zhang et al., 2006). The

265 weighted-average SST (0–30 m) based on chlorophyll concentration is 25.7°C, which is
266 only 0.6°C lower than the mean annual temperature at 0–30 m (26.3°C). These
267 observations suggest that the $U^{K'}_{37}$-derived temperature reflects the mean annual SST at the
268 study site.

269 The core-top temperature based on $TEX_{86}^{H}$ is 28.1°C. This temperature is 1.5°C higher
270 than the mean annual SST (26.6°C; NOAA, 1998) and agrees with the SST in May and
271 September–October at this site (~28.0°C and ~27.7-28.6°C, respectively; NOAA, 1998). It
272 has been reported that the GDGT concentration in surface waters is higher during
273 non-blooming seasons in the North Sea and the Bermuda Rise (Wuchter et al., 2005). By
274 analogy with this case, although there is no information on the production season and depth
275 of GDGTs at the study site, it is reasonable to infer that GDGT are produced during the
276 summer season when blooms cease. We infer, therefore, that the $TEX_{86}^{H}$-derived
277 temperature reflects the SST weighted in warmer seasons at the study site.

278 The $U^{K'}_{37}$-derived temperature shows a different temporal evolution in comparison with
279 $TEX_{86}^{H}$-derived temperatures (Figs. 3A and 3B). We interpret $U^{K'}_{37}$-derived temperatures as
280 reflecting mean annual SST (Shintani et al., 2008). The average of summer and winter
281 SSTs estimated by a regional Imbrie–Kipp transfer function method (FP-12E; Thompson,
282 1981) of planktonic foraminifera in core 19740 (Wang et al., 1999b) agreed with
283 $U^{K'}_{37}$-derived temperature in core MD97-2146 (Fig. 3B), supporting this interpretation.

284 On the other hand, we interpret the $TEX_{86}^{H}$-derived temperature estimate at a core top
285 sediment sample to reflect the SST weighted in warmer seasons. The $TEX_{86}^{H}$-derived
286 temperatures in core MD97-2146 range between summer and annual mean SSTs estimated
287 by a transfer function method in core 19740 (Wang et al., 1999b) during the Holocene,
288 whereas they agree with the annual mean SSTs during the last glacial period between 18

289 and 27 ka (Fig. 3A). There are three possible interpretations of this phenomenon, such as 1)
290 the seasonal shift of GDGT production, 2) the overestimation of temperature change by
291 $TEX_{86}^{H}$, and 3) the underestimation of temperature change by $U_{37}^{K'}$ and transfer function
292 approaches.

293 First, the seasonal shift of GDGT production from warmer seasons to cooler seasons is
294 one of the candidate mechanisms accounting for larger variation in $TEX_{86}^{H}$-derived
295 temperature than in $U_{37}^{K'}$- and transfer function-derived mean annual SSTs. The GDGT
296 concentration in surface waters has been reported to be higher during non-blooming
297 seasons in the North Sea and the Bermuda Rise (Wuchter et al., 2005). If the phytoplankton
298 blooms shifted to warmer seasons due to the temperature limitation of phytoplankton
299 growth, the production of GDGTs would decrease in warmer seasons, and $TEX_{86}^{H}$ should
300 reflect the SST in cooler seasons.

301 Second, the overestimation of temperature change by $TEX_{86}^{H}$ is possible due to
302 calibration at this stage. Global core top calibration was revised by increasing surface
303 sediment samples (Schouten et al., 2002; Kim et al., 2008; 2010). The most recently
304 revised calibration gives smaller temperature change than did previous versions. Kim et al.
305 (2010) also pointed out that crenachaeotal ecology is different between subpolar and
306 subtropical water masses and may have different responses to temperature change. If a
307 water mass is displaced by another water mass, a complex response to temperature change
308 results. Caution is necessary when discussing the degree of variation in $TEX_{86}$-derived
309 temperature until temperature calibration is practically established.

310 Last, possible underestimations of temperature change by $U_{37}^{K'}$ and the transfer
311 function methods are not negligible. Because the production of coccolithophores is
312 temperature dependant (Conte et al., 1998), the season of maximum production may have

313 shifted to the warmest times of year, during periods of decreasing mean annual SST. It is
314 thus possible that the drop in $U^{K'}_{37}$-derived temperatures may be an underestimate.
315 Temperature at core 17940 was estimated by a regional Imbrie–Kipp method (Wang et al.,
316 1999b). Chen et al. (2005) compared the results of temperature estimates by different
317 transfer function techniques and found that the Imbrie–Kipp method tends to show smaller
318 temperature variation than those obtained by other methods. In addition, Steinke et al.
319 (2008) showed that transfer function methods give smaller glacial–interglacial variation in
320 SST compared with those inferred by geochemical proxies in the SCS because there are
321 no-modern analog planktonic foraminiferal faunas in the glacial SCS. These lines of
322 evidence suggest that glacial cooling may be underestimated by $U^{K'}_{37}$ and transfer function
323 methods.

324 It is now not clear which of the above mechanism is critical in causing the difference
325 between proxies. Further comparison studies of proxies are necessary to answer this
326 question.

327 The $TEX_{86}^{H}$-derived temperatures in core MD97-2146 generally agree with the
328 foraminiferal Mg/Ca-derived temperatures at ODP Site 1145, located ~100 km south of
329 Site MD97-2146 (Fig. 3; Oppo and Sun, 2005), but the disagreement is again observed in
330 the period between 18 ka and 15 ka (Figs. 3A and 3C). The cooling observed in
331 $TEX_{86}^{H}$-derived temperatures during the 15–18 ka could be somehow overestimated, as
332 other proxies do not indicate such a cooling. The anomalies of $TEX_{86}^{H}$-derived
333 temperatures are potentially attributable to seasonal shift of GDGT production, changes in
334 the GDGT production depth, lateral transport of GDGTs and additional contribution of
335 GDGTs by archaeal communities other than Marine Group I Crenarchaeota (Kim et al.,
336 2008). There is now no evidence to support the above possibilities, but they must be

337 considered by further studies.

338 The changing pattern of $TEX_{86}^{H}$-derived temperature record from 15 to 10 ka shows a
339 good correspondence to the millennial-scale pattern of stalagmite oxygen isotopes from the
340 Hulu Cave, eastern central China (Wang et al., 2001), and the Dongge Cave, south China
341 (Yuan et al., 2004). The variation in stalagmite $\delta^{18}O$ is thought to reflect changes in the
342 relative abundance of summer vs. winter precipitation: low values correspond to larger
343 contributions of summer precipitation due to an increased intensity of the East Asian
344 summer monsoon. The correspondence of the pattern of change between $TEX_{86}^{H}$-derived
345 temperature at the study site and Chinese stalagmite $\delta^{18}O$ suggests that changes in
346 $TEX_{86}^{H}$-derived temperature in this period reflected atmospheric and oceanic
347 reorganization on a millennial timescale.

348

349 *5.2. Inflow of terrestrial organic matter to the study site*

350 The total long-chain n-alkane concentration decreases in the interval from 15 ka to 13 ka
351 (Fig. 4). The similar trend of long-chain n-alkane concentration was previously reported in
352 nearby core 17940 (Pelejero, 2003; Kienast et al., 2010) and was attributed to the
353 emergence and flooding of the shelves caused by sea level variations, together with SCS
354 SSTs, have a clear dependency on the Northern Hemisphere climate evolution.

355 In this study, the long-chain n-alkanes were separately determined as higher plant-derived
356 n-alkanes and lithic n-alkanes. The long-chain n-alkanes are mainly of higher plant origin
357 before ~14–15 ka and a mixture of higher plant and lithic origins after ~14–15 ka (Fig. 4A).
358 The sudden decrease of higher plant n-alkane concentration was accompanied by a
359 decrease in the ratio of long-chain to short-chain n-fatty acids (Fig. 4B). These observations
360 suggest that the relative contribution of fresh higher plants decreased and that the

361 contribution of mature organic matter derived from sedimentary rocks increased between
362 14 and 15 ka, indicating a drastic change in sediment provenance at this time.
363 Wang et al. (1999a) showed that the median grain size of silt and the total modal grain
364 size of sediments decreased, while the clay content increased, at the onset of the
365 Bølling-Allerød (B-A) period at core site 17940. This decrease in the average grain size
366 and increase in clay content was interpreted as indicating a decrease in the supply of dust
367 and an increase in the supply of fine fluvial material from the Pearl River at ~14.5 ka.
368 Wang et al. (1999a) stressed that this change reflects the shift from a winter
369 monsoon-dominated glacial regime to a summer monsoon-dominated Holocene regime.
370 Tamburini et al. (2003) found higher illite content in SCS sediment during the Holocene,
371 while smectite and kaolinite were elevated during glacial periods. Because illite is
372 abundant in sediments derived from the Asian continent, and smectite and kaolinite are
373 relatively abundant in sediments from the southern tropical islands, the change in
374 clay-mineral composition may reflect changes in sediment provenance. Studies on modern
375 sediments indicate that reworking of material from the Pearl River (Wang et al., 1999a) and
376 current transport from the East China Sea through the open Taiwan Strait (Chen, 1978)
377 should be considered the main transport mechanism responsible for clay and mineral
378 distribution in the northern SCS (Tamburini et al., 2003). The low illite content during the
379 last glacial period was attributed to the interruption of the input of illite-rich material from
380 the East China Sea shelf when a low sea level stand closed the Taiwan Strait (Tamburini et
381 al., 2003).
382 The sill depth of the Taiwan Strait is ~70 m, and a marine connection was established by
383 ~13 ka, later than the decreases of fresh higher plant-derived n-alkane and n-fatty acids
384 (Fig. 4). This implies that the opening of the Taiwan Strait was not a cause of the low

385 content of higher plant biomarkers.

386 On the other hands, the decrease of fresh higher plant n-alkanes at 15 ka coincides with
387 the increase of the Asian summer monsoon intensity recorded in Chinese stalagmites
388 (Wang et al., 2001; Yuan et al., 2004). The greater content of fresh higher plant n-alkanes
389 and long-chain n-fatty acids in sediments prior to 14–15 ka is attributable to enhanced
390 aeolian transportation and/or arid environments in South China (Sun and Li, 1999).
391 Enhanced precipitation due to the intensified East Asian summer monsoon after ~14–15 ka
392 increased the erosion of sub-aerially exposed sedimentary rocks, increasing the relative
393 proportion of lithic n-alkanes.

394

395 *5.3. Paleoenvironment after 2 ka*

396 The ACL is significantly higher in the Oldest Dryas period and after 2 ka (Fig. 4). In
397 general, ACL values are higher in herbs than in trees (e.g., Vogts et al., 2009). A pollen
398 study at the site of core 17940, near our study site, showed that herb pollen (e.g., *Artemisia*,
399 *Gramineae*, and *Cyperaceae*) was abundant during the Oldest Dryas period, due to the cold
400 and dry climate, and decreased during the Bølling-Allerød period (Sun and Li, 1999). The
401 high ACL in the Oldest Dryas period is consistent with the high abundance of herb pollen.
402 Fern spores significantly increased after 1.4 ka in core 17940, possibly due to human
403 activity (Sun and Li, 1999). This increase corresponds to the increase of ACL in the study
404 core. There is one report for a fern *Hydrilla verticillate* having high ACL (Chikaraishi and
405 Naraoka, 2003), but we do not fully understand the ACL in ferns. Thus we cannot attribute
406 this change to the increase of ferns; future investigations of fern ACLs are necessary. The
407 core site is proximal to South China and is thus in an ideal position to trace environmental
408 changes by human activities in historical times. Further applications of new techniques will

409 contribute to better understanding the environmental changes in South China.

410

411 **Conclusions**

412 We applied $TEX_{86}^{H}$ paleothermometry to sediment from the SCS and demonstrated
413 measurable SST variations over the past 28 kyr. The $TEX_{86}^{H}$-derived temperature of a
414 core-top sample corresponds to the SSTs in warmer seasons. The glacial–interglacial
415 contrast in $TEX_{86}^{H}$-derived temperature is almost the same as that in foraminiferal Mg/Ca
416 ratio-derived temperature, but it is larger than those in $U_{37}^{K'}$ and transfer function-derived
417 temperatures. The similar variation in $TEX_{86}^{H}$-derived temperature at the study site and
418 Chinese stalagmite $\delta^{18}O$ during the last deglaciation suggests that changes in
419 $TEX_{86}^{H}$-derived temperature in this period reflected atmospheric and oceanic
420 reorganization on a millennial timescale.

421 We also examined terrestrial biomarkers such as n-alkanes and n-fatty acids that show a
422 remarkable change from abundant fresh higher plants to the mixture of fresh higher plants
423 and mature organic matter at 14–15 ky BP. We consider this is a result of a considerable
424 change in sediment delivery at that time. Terrestrial organic matter was presumably
425 supplied by enhanced aeolian transportation prior to 14–15 ka, with the contribution from
426 river discharge becoming more important thereafter presumably due to intensified summer
427 monsoon.

428

429 *Acknowledgements:* We thank shipboard members of IMAGES 1997 cruise. We also thank
430 Ellen Hopmans and Stefan Schouten (Royal Netherlands Institute for Sea Research) for
431 kindly giving us advice about GDGT and $TEX_{86}$ analysis. Thanks go to Tatsufumi Okino,
432 Yusuke Izawa, Masao Minagawa, and Tomohisa Irino (Hokkaido University) for help with

analysis. Comments by four anonymous reviewers improved this manuscript. This study was supported by a grant-in-aid for Scientific Research (A) the Japan Society for the Promotion of Science, No. 19204051 (to MY).

## Reference

Bray, E.E., Evans, E.D., 1961. Distribution of n-paraffins as a clue to the recognition of source beds. Geochimica et Cosmochimica Acta 22, 2–9.

Chen, P.-Y., 1978. Minerals in bottom sediments of the South China Sea. Geological Society of America Bulletin 89, 211–222.

Chen, M.-T., Huang, C.-Y., 1998. Ice-volume forcing of winter monsoon climate in the South China Sea. Paleoceanography 13, 622–633.

Chen, M.-T., Beaufort, L., the Shipboard Scientific Party of the IMAGES III/MD106-IPHIS Cruise (Leg II), 1998. Exploring Quaternary variability of the East Asian monsoon, Kuroshio Current, and the Western Pacific warm pool systems: high-resolution investigations of paleoceanography from the IMAGES III/MD106-IPHIS cruise. Terrestrial, Atmospheric and Oceanic Sciences 9, 129–142.

Chen, M.-T., Shiau, L.-J., Yu, P.-S., Chiu, T.-C., Chen, Y.-G., Wei, K.-Y., 2003. 500 000-Year records of carbonate, organic carbon, and foraminiferal sea surface temperature from the southeastern South China Sea (near Palawan Island). Palaeogeography, Plaeoclimatology, Palaeoecology 197, 113–131.

Chen, M.-T., Huang, C.-C., Pflaumann, U., Waelbroeck, C., Kucera, M., 2005, Estimating glacial western Pacific sea surface temperature: methodological overview and data compilation of surface sediment planktic foraminifer faunas. Quaternary Science Reviews 24, 1049–1062.

457 Chikaraishi, Y., Naraoka, H., 2003. Compound-specific δD-$\delta^{13}$C analyses of n-alkanes
458 extracted from terrestrial and aquatic plants. Phytochemistry, 63, 361–371.
459 Conte, M.H., Thompson, A., Lesley, D., Harris, R P., 1998. Genotypic and physiological
460 influences on the alkenone/alkenoate versus growth temperature relationship in
461 *Emiliania huxleyi* and *Gephyrocapsa oceanica*. Geochimica et Cosmochimica Acta
462 62, 51–68.
463 Eglinton, G., Hamilton, R.J., 1967. Leaf epicuticular waxes. Science 156, 1322–1355.
464 Hopmans, E.C., Schouten, S., Pancost, R., van der Meer, M.T.J., Sinninghe Damsté, J.S.,
465 2000. Analysis of intact tetraether lipids in archaeal cell material and sediments by
466 high performance liquid chromatography/atmospheric pressure chemical ionization
467 mass spectrometry. Rapid Communications in Mass Spectrometry 14, 585–589.
468 Hopmans, E.C., Weijers, J.W.H., Schefuß, E., Herfort, L., Sinninghe Damsté, J.S.,
469 Schouten, S., 2004. A novel proxy for terrestrial organic matter in sediments normalized
470 on branched and isoprenoid tetraether lipids. Earth and Planetary Science Letters 224,
471 107–116.
472 Huang, C.-Y., Liew, P.-M., Zhao, M., Chang, T.-C., Kuo, C.-M., Chen, M.-T., Wang, C.-H.,
473 Zheng, L., 1997a. Deep sea and lake records of the Southeast Asian paleomonsoons
474 for the last 25 kyrs. Earth and Planetary Science Letters 146, 59–72.
475 Huang, C.-Y., Wu, S.-F., Zhao, M., Chen, M.-T., Wang, C.-H., Tu, X., Yuan, P.B., 1997b.
476 Surface ocean and monsoon climate variability in the South China Sea since last
477 glaciation. Marine Micropaleontology 32, 71–94.
478 Kienast, M., Steinke, S, Stattegger, K., Calvert, S.E., 2001. Synchronous tropical South
479 China Sea SST changes and Greenland warming during deglaciation. Science 291,
480 2132–2134.

481 Kienast, M., Hanebuth, T.J.J., Pelejero, C., Steinke, S., 2010. Synchroneity of metwater
482 pulse 1a and the Bølling warming: New evidence from the South China Sea. Geology,
483 31, 67–70.
484 Kim, J.-H., Schouten, S., Hopmans, E.C., Donner, B., Sinninghe Damsté, J.S., 2008.
485 Global sediment core-top calibration of the TEX86 paleothermometer in the ocean.
486 Geochimica et Cosmochimica Acta 72, 1154–1173.
487 Kim, J-H., van der Meer, J., Schouten, S., Helmke, P., Willmott, V., Sangiorgi, F., Koc, N.,
488 Hopmans, E.C., Sinninghe Damsté, J.S., 2010. New indices and calibrations derived
489 from the distribution of crenarchaeal isoprenoid tetraether lipids: Implications for past
490 sea surface temperature reconstructions. Geochimica et Cosmochimica Acta, 74,
491 4639–4654
492 Kvenvolden, K.A., 1967. Normal fatty acids in sediments. Journal of The American Oil
493 Chemists' Society 44, 628–636.
494 Lambeck, K., Yokoyama, Y., Purcell, T., 2002. Into and out of the Last Glacial Maximum:
495 sea level change during Oxygen Isotope Stages 3 and 2. Quaternary Science Reviews
496 21, 343–360.
497 Lin, D.-C., Liu, C.-H., Fang, T.-H., Tsai, C.-H., Murayama, M., Chen, M.-T., 2006.
498 Millennial-scale changes in terrestrial sediment input and Holocene surface
499 hydrography in the northern South China Sea. Palaeogeography, Palaeoclimatology,
500 Palaeoecology 236, 56–73.
501 NOAA, 1998. http://iridl.ldeo.columbia.edu/SOURCES/.NOAA/.NODC/.WOA98/
502 Oppo, D.W., Sun, Y., 2005. Amplitude and timing of sea-surface temperature changes in
503 the northern South China Sea: Dynamic link to the East Asian monsoon. Geology 33,
504 785–788.

505 Pelejero, C., Grimalt, J.O., Heilig, S., Kienast, M., Wang, L., 1999a. High-resolution $U_{37}^{K'}$
506 temperature reconstructions in the South China Sea over the past 220 kyr.
507 Paleoceanography 14, 224–231.
508 Pelejero, C., Grimalt, J.O., Sarnthein, M., Wang, L., Flores, J.-A., 1999b. Molecular
509 biomarker record of sea surface temperature and climatic change in the South China
510 Sea during the last 14000 years. Marine Geology 156, 109–121.
511 Pelejero, C., 2003. Terrigenous n-alkane input in the South China Sea: high-resolution
512 records and surface sediments. Chemical Geology, 200, 89–103.
513 Prahl, F.G., Muehlhausen, L.A., Zahnle, D.L., 1988. Further evaluation of long-chain
514 alkenones as indicators of paleoceanographic conditions. Geochimica et
515 Cosmochimica Acta 52, 2303–2310.
516 Reimer, P.J., Baillie, M.G.L., Bard, E., Bayliss, A., Beck, J.W., Bertrand, C.J.H., Blackwell,
517 P.G., Buck, C.E., Burr, G.S., Cutler, K.B., Damon, P.E., Edwards, R.L., Fairbanks,
518 R.G., Friedrich, M., Guilderson, T.P., Hogg, A.G., Hughen, K.A., Kromer, B.,
519 McCormac, F.G., Manning, S.W., Ramsey, C.B., Reimer, R.W., Remmele, S.,
520 Southon, J.R., Stuiver, M., Talamo, S., Taylor, F.W., van der Plicht, J., Weyhenmeyer,
521 C.E., 2004. IntCal04 Terrestrial radiocarbon age calibration, 26 - 0 ka BP.
522 Radiocarbon 46, 1029–1058.
523 Schouten, S., Hopmans, E.C., Schefuß, E., Sinninghe Damsté, J.S., 2002. Distributional
524 variations in marine crenarchaeotal membrane lipids: a new tool for reconstructing
525 ancient sea water temperatures? Earth and Planetary Science Letters 204, 265–274.
526 Schouten, S, Huguet, C., Hopmans, E.C., Kienhuis, M.V.M., Sinninghe Damsté, J.S., 2007.
527 Analytical methodology for $TEX_{86}$ paleothermometry by high performance liquid
528 chromatography/atmospheric pressure chemical ionization-mass spectrometry.

529 Analytical Chemistry 79, 2940–2944.
530 Shintani, T., Yamamoto, M., Chen, M.-T., 2008. Slow warming of the northern South
531 China Sea during the last deglaciation. Terrestrial, Atmospheric and Oceanic
532 Sciences, 19, 341–346.
533 Steinke, S., Kienast, M., Groeneveld, J., Lin, J.-C., Chen, M.-T., Rendle-Bühring, R., 2008.
534 Proxy dependence of the temporal pattern of deglacial warming in the tropical South
535 China Sea: toward resolving seasonality. Quaternary Science Reviews 27, 688–700.
536 Sun, X., Li, X., 1999. A pollen record of the last 37 ka in deep sea core 17940 from the
537 northern slope of the South China Sea, Marine Geology 156, 227–244.
538 Tamburini, F., Adatte, T., Föllmi, K., Berasconi, S.M., Steinmann, P., 2003. Investigation
539 the history of East Asian monsoon and climate during the last glacial–interglacial
540 period (0-140 000 years): mineralogy and geochemistry of ODP Sites 1143 and 1144,
541 South China Sea. Marine Geology 201, 147–168.
542 Thompson, P.R., 1981. Planktonic foraminifera in the Western North Pacific during the past
543 150,000 years: comparison of modern and fossil assemblages. Palaeogeography,
544 Palaeoclimatology, Palaeoecology, 35, 241–279.
545 Tissot, B.P., Welte, D.H., 1984. *Petroleum Formation and Occurrence*, 2nd. ed.,
546 Springer-Verlag, Berlin.
547 Turich, C., Freeman, K.H., Bruns, M.A., Conte, M., Jones, A.D., Wakeham, S.G., 2007.
548 Lipids of marine Archaea: Patterns and provenance in the water-column and sediments.
549 Geochimica et Cosmochimica Acta 71, 3272–3291.
550 Vogts, A., Moossen, H., Rommerskirchen, F., Rullkötter, J., 2009. Distribution patterns and
551 stable carbon isotopic composition of alkanes and alkan-1-ols from plant waxes of
552 African rain forest and savanna $C_3$ species. Organic Geochemistry 40, 1037–1054.

553 Wang, L., Wang, P., 1990. Late Quaternary paleoceanography of the South China Sea:
554 Glacial–interglacial contrasts in an enclosed basin. Paleoceanography 5, 77–90.
555 Wang, P., Wang, L., Bian Y., Jian, Z., 1995. Late Quaternary paleoceanography of the
556 South China Sea: surface circulation and carbonate cycles. Marine Geology 127,
557 145–165.
558 Wang, L., Sarnthein, M., Grootes, P.M., Erlenkeuser, H., 1999a. Millennial reoccurrence of
559 century-scale abrupt events of East Asian monsoon: A possible heat conveyor for the
560 global deglaciation. Paleoceanography 14, 725–731.
561 Wang, L., Sarnthein, M., Erlenkeuser, H., Grimalt, J.O., Grootes, P.M., Heilig, S., Ivanova,
562 E., Kienast, M., Pelejero, C., Pflaumann, U., 1999b. East Asia monsoon climate
563 during the late Pleistocene: high-resolution sediment records from the South China
564 Sea. Marine Geology 156, 245–284.
565 Wang, Y. J., Cheng, H., Edwards, R.L., An, Z.S., Wu, J Y., Shen, C.-C., Dorale, J.A., 2001.
566 A High-Resolution Absolute-Dated Late Pleistocene Monsoon Record from Hulu
567 Cave, China. Science 294, 2345–2348.
568 Wuchter, C., Schouten, S., Coolen, M.J.L., Sinninghe Damsté, J.S., 2004.
569 Temperature-dependent variation in the distribution of tetraether membrane lipids of
570 marine Crenarchaeota: Implications for $TEX_{86}$ paleothermometry. Paleoceanography
571 19, PA4028.
572 Wuchter, C., Schouten, S., Wakeham, S.G., Sinninghe Damsté, J.S., 2005. Temporal and
573 spatial variation in tetraether membrane lipids of marine Crenarchaeota in particulate
574 organic matter: Implications for $TEX_{86}$ paleothermometry. Paleoceanography 20,
575 PA3013.
576 Wyrtki, K., 1961. Physical oceanography of the southeast Asia waters. In Scientific Results

577 of Maritime Investigations of the South China Sea and the Gulf of Thailand
578 1959–1961, Naga Rep. 2, Scripps Institute of Oceanography, La Jolla, Calif. U.S.A.
579 Yamamoto，M., Polyak, L., 2009. Changes in terrestrial organic matter input to the
580 Mendeleev Ridge, western Arctic Ocean, during the Late Quaternary. Global and
581 Planetary Change 68, 30–37.
582 Yuan, D., Cheng, H., Lawrence, E.R., Dykoski,C.A., Kelly, M.J., Zhang, M., Qing, J., Lin,
583 Y., Wang, Y., Wu, J., Dorale, J.A., An, Z., Cai, Y., 2004. Timing, Duration, and
584 Transitions of the Last Interglacial Asian Monsoon. Science 304, 575–578.
585 Zhang, C., Hu, C., Shang, S., Frank E., Karger, M., Li, Y., Dai, M., Huang, B., Ning, X.,
586 Hong, H., 2006. Bridging between SeaWiFS and MODIS for continuity of
587 chlorophyll-a concentration assessments off Southeastern China. Remote Sensing of
588 Environment 102, 250–263.
589 Zhao, M., Huang, C.-Y., Wang, C.-C., Wei, G. 2006. A millennial-scale $U_{37}^{K'}$ sea surface
590 temperature record from the South China Sea (8°N) over the last 150 kyr: Monsoon
591 and sea-level influence. Palaeogeography, Palaeoclimatology, Palaeoecology 236,
592 39–55.
593

**Figure captions**

Fig. 1. Map showing the locations of core MD97-2146 and other cores referred to in this paper.

Fig. 2. Depth and seasonal variation of water temperatures at the study site (Compiled data from NOAA, 1998). “J” to ”D” means January to December.

Fig. 3. (A) $TEX_{86}^{H}$ and (B) $U^{K'}_{37}$-derived temperatures in core MD97-2146, and (C) Mg/Ca-derived SST in ODP Site 1145 (Oppo and Sun, 2005) during the last 28 kyr. The summer, winter and annual mean SSTs estimated by a regional Imbrie–Kipp transfer function method (FP-12E; Thompson, 1981) of planktonic foraminifera in core 19740 (Wang et al., 1999b) are also shown in each panel.

Fig. 4. (A) Concentrations of total, higher plant, and lithic long-chain $C_{25}$-$C_{33}$ n-alkanes, and the CPI and ACL of n-alkanes. (B) Concentrations of total ($C_{14}$-$C_{34}$), short-chain ($C_{14}$-$C_{18}$), and long-chain ($C_{26}$-$C_{34}$) n-fatty acids, and the CPI of n-fatty acids and abundance ratio of long-chain to short-chain (L/S ratio) n-fatty acids in core MD97-2146 during the last 28 kyr. (C) Reconstructed sea level (Lambeck *et al*., 2002) and the sill depths of straits to the East China Sea, the Sulu Sea, the Indian Ocean and the Java Sea (Wyrtki, 1961).


614

615 Fig. 1

616

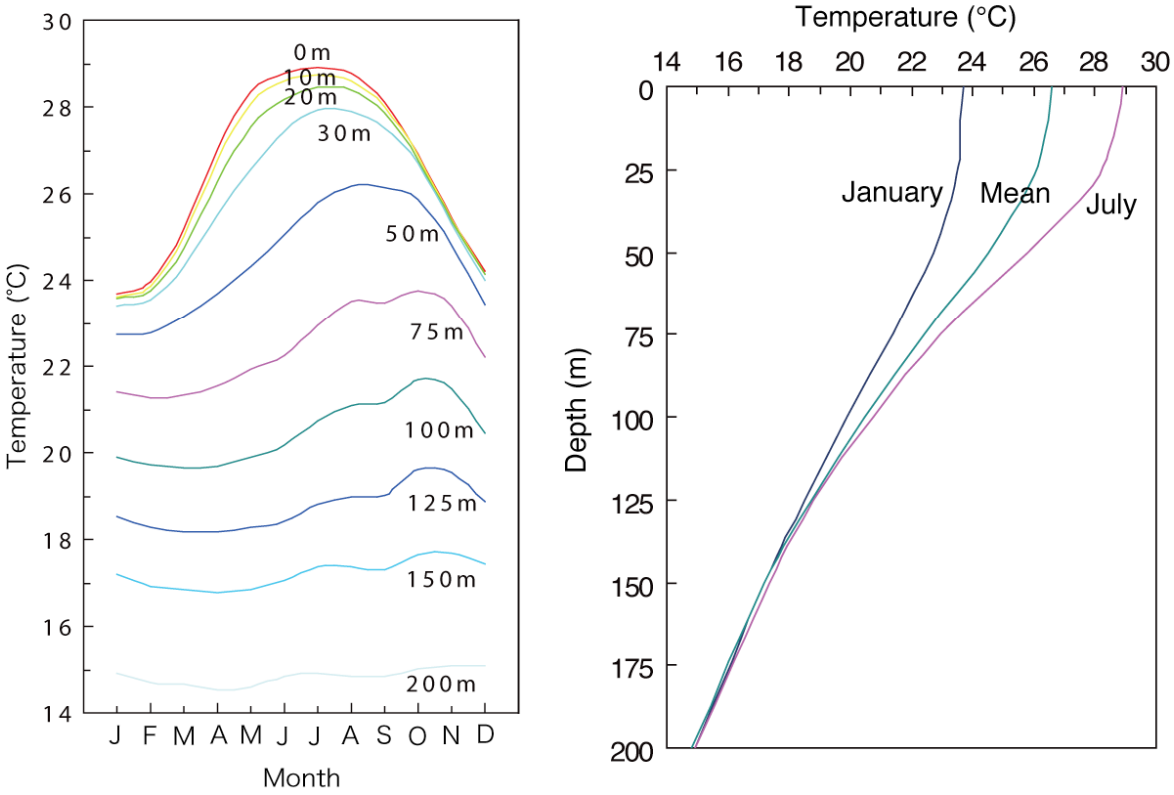


617

618

619 Fig. 2

620

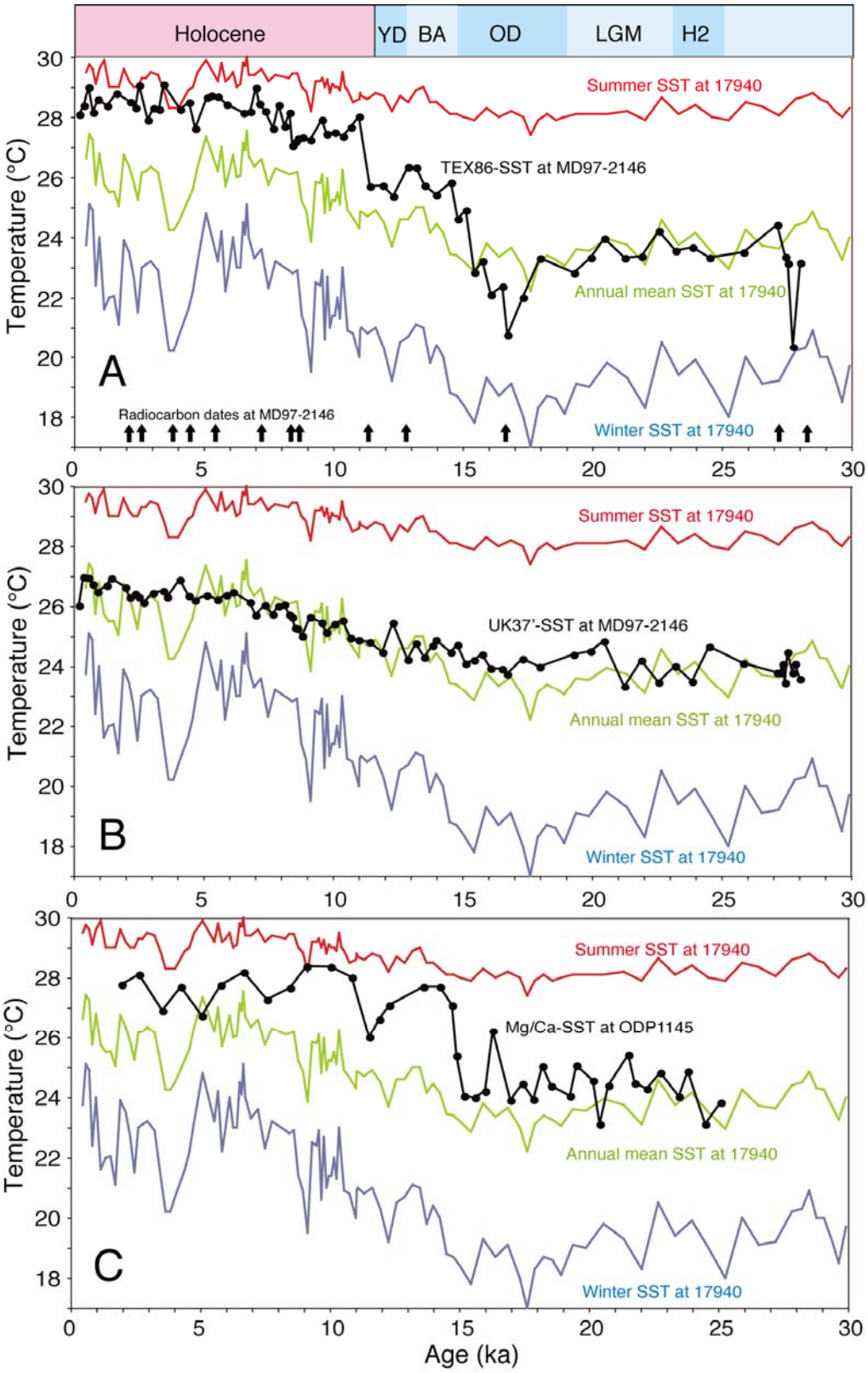


621

622

623 Fig. 3

624

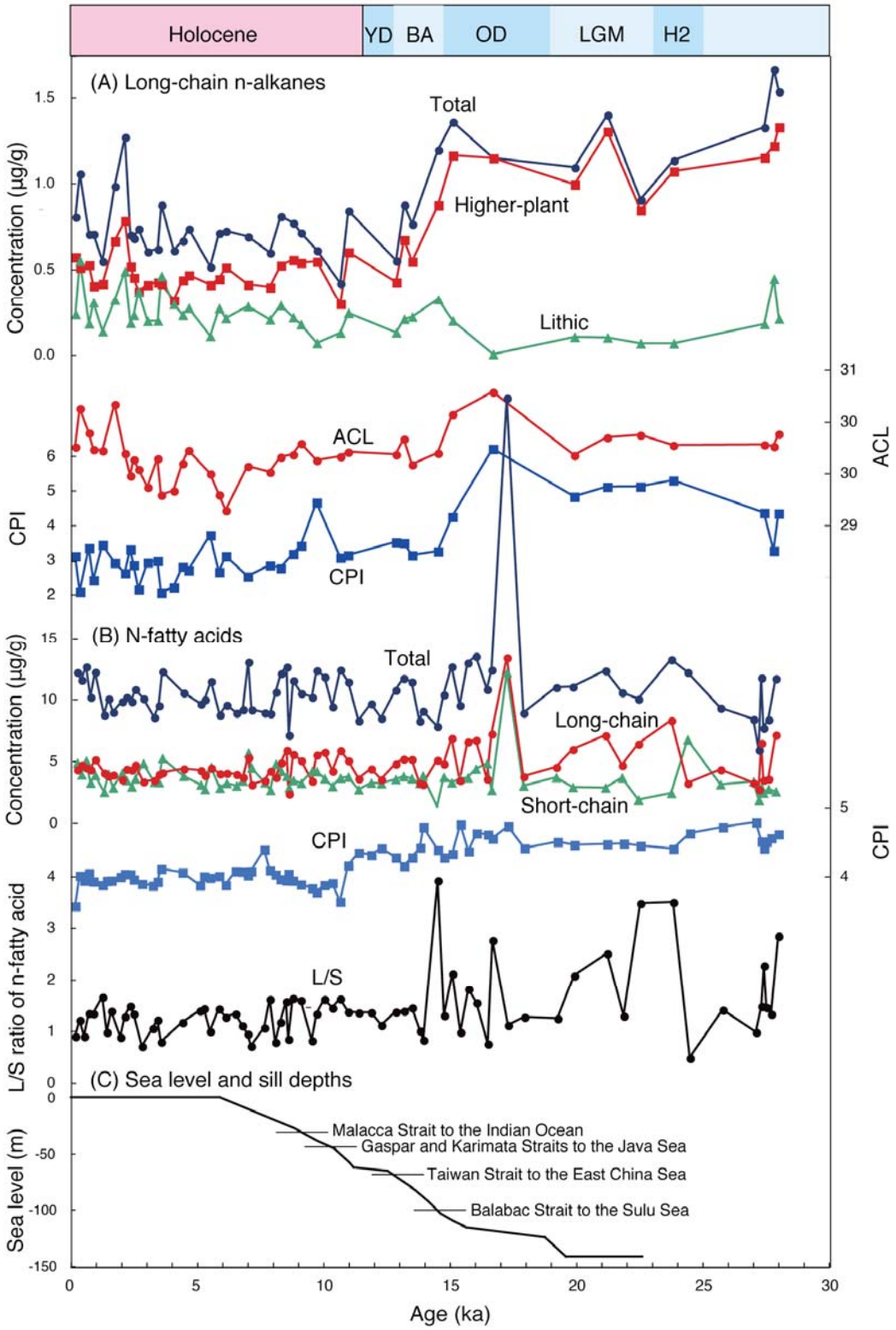


625

626

627 Fig. 4